



A novel theoretical study of thermally-induced reaction and vibration dynamics of methanol dissociative adsorption onto Si(001) surface

Journal:	<i>RSC Advances</i>
Manuscript ID	RA-ART-10-2015-022759.R1
Article Type:	Paper
Date Submitted by the Author:	14-Dec-2015
Complete List of Authors:	Lee, Yung-Ting; Tamkang University, Chemistry; Korea Advanced Institute of Science and Technology, Physics Lin, Jyh Shing; Tamkang University,
Subject area & keyword:	Simulations < Physical

A novel theoretical study of thermally-induced reaction and vibration dynamics of methanol dissociative adsorption onto Si(001) surface

Yung Ting Lee^{1,2} and Jyh Shing Lin^{1*}

¹Department of Chemistry, Tamkang University

Tamsui, New Taipei City 25137, Taiwan

²Department of Physics, Korea Advanced Institute of Science and Technology,

Daejeon 305-701, Korea

Abstract

The thermally-induced reaction and vibration dynamics of methanol ($\text{CH}_3\text{OH}_{(\text{g})}$) dissociative adsorption onto the Si(001) surface have been studied by combining density functional theory (DFT)-based molecular dynamics (DFTMD) simulations with a molecular adsorption sampling scheme and a wavelet transform for investigating the reaction pathways and corresponding vibrational spectra. Based on the simulated results, $\text{CH}_3\text{OH}_{(\text{g})}$ firstly approaches the Si(001) surface to interact with the buckled-down Si atom at the temperature from 100 K to 300 K, and then the O-H bond of $\text{CH}_3\text{OH}_{(\text{ads})}$ breaks within 10 picoseconds only at 300 K due to the elongation of the O-H bond. Furthermore, the time-resolved vibrational spectrum constructed by a wavelet transform of structural coordinate auto-correlation function (WT-SCAF) illustrates that the O-H stretching mode of $\text{CH}_3\text{OH}_{(\text{ads})}$ shifts to below 3400 cm^{-1} when the H atom of the O-H bond is closer to the buckled-up Si atom of

the adjacent dimers. This is due to the fact that the noticeable attractive force between the H atom of the O-H bond and the dangling bond at the buckled-up Si atom of the adjacent dimers prompts the O-H bond to break and then leads to both CH₃O and H species adsorbed on the buckled-down and buckled-up Si atoms, respectively.

Introduction

Recently, the dissociative adsorption of alcohols onto semiconductor surfaces has attracted considerable attention for solvent cleaning of silicon wafers and silica production.¹⁻² For example, methanol is one typical example of organic aqueous solvents to remove contaminants on the silicon surface³ and ethanol is used in the processing steps in the preparation of silicon surfaces.^{4,5} It's worth to note that these reaction processes involve the forming of the Si-O bond and the breaking of the O-H bond based on experimental results using Fourier transform reflection-absorption infrared spectroscopy (FT-RAIRS)^{6,7}, high-resolution photoemission^{8,9}, and Auger electron spectroscopy¹⁰. Therefore, the study of the reaction dynamics of molecular dissociative adsorption on the semiconductor surface is of great importance to understand the reaction mechanisms and corresponding dynamic behaviors at different temperatures and to help further development of semiconductor device fabrication techniques.

The early research work studied by FT-RAIRS⁶, infrared spectra (IR) of methanol ($\text{CH}_3\text{OH}_{(\text{ads})}$) adsorbed on the epitaxial grown Si(001)-2x1 surface showed that (1) the C-O stretching mode (1050 cm^{-1}) and CH_3 rocking mode (1179 cm^{-1}) of $\text{CH}_3\text{OH}_{(\text{ads})}$ appear from 100 K to 550 K, (2) the Si-H stretching mode of 2090 cm^{-1} is observed after heating the sample to 150 K indicating the breaking of O-H bond and the forming of Si-H bond, and (3) finally no other stretching mode have been observed above 600 K. It clearly illustrates that $\text{CH}_3\text{OH}_{(\text{g})}$ first adsorbs on the Si(001) surface, then breaks the O-H bond and finally forms the Si-H bond as substrate temperature increases above 150 K. It is consistent with the result of the O-H bond breakage of $\text{CH}_3\text{OH}_{(\text{ads})}$ adsorbed on the porous silicon at 300 K³. Similarly, in

ethanol adsorption, ethanol ($\text{CH}_3\text{CH}_2\text{OH}$) adsorbed on Si(001) surface first breaks its O-H bond to form ethoxide ($\text{CH}_3\text{CH}_2\text{O}$) species and the Si-H stretching mode of 2089 cm^{-1} appears in IR spectrum at 219 K .⁷ Furthermore, Casaletta et al. also showed that the ionization peak of $\sigma_{\text{O-H}}$ bond of $\text{CH}_3\text{OH}_{(\text{ads})}$ adsorbed on the Si(001)- 2×1 surface is missing in valence band and two surface-related components, i.e. Si-H and Si-OCH₃, upon adsorption appears in Si 2p photoemission spectra at room temperature by high-resolution synchrotron radiation photoemission.⁸ This study indicates that the O atom of $\text{CH}_3\text{OH}_{(\text{ads})}$ forms the bond with the Si atom rather than the C atom of $\text{CH}_3\text{OH}_{(\text{ads})}$ does because the O atom of $\text{CH}_3\text{OH}_{(\text{g})}$ can provide one lone pair of electrons for bonding with the buckled-down Si atom.

Based on cluster models of static calculations, Lu et al. have proposed the reaction pathway of the O-H bond breaking of $\text{CH}_3\text{OH}_{(\text{ads})}$ at the same dimer and corresponding activation barrier about 0.2 eV .¹¹ Kato et al. have investigated that the C-O bond breaking of $\text{CH}_3\text{OH}_{(\text{ads})}$ requires 1.2 eV more activation energy than the O-H bond breaking.¹² In addition, using density functional theory slab calculations, Carbone et al. have shown that methanol and methoxide (CH_3O) adsorbed on Si(001) surface are energetically favorable on the top site of the Si dimer.^{13,14} Miotto et al. point out that the cleavage of the O-H bond of $\text{CH}_3\text{OH}_{(\text{ads})}$ is easier than that of the C-H bond.^{15,16} Although various adsorbed structures and corresponding reaction pathway along methanol dissociative adsorption have been discussed, some questions remain unanswered including (1) how the O-H bond of $\text{CH}_3\text{OH}_{(\text{ads})}$ interacts with either the same Si dimer or the adjacent Si dimer, (2) why the O-H stretching mode exhibits a broadening peak rather than a sharp peak, and (3) how the effect of temperature leads to the dissociation of the O-H bond of $\text{CH}_3\text{OH}_{(\text{ads})}$.

In this study, therefore, the DFTMD calculations combined with a “molecular adsorption sampling” (MAS) scheme¹⁷ are performed to simulate the reaction dynamics of methanol dissociative adsorption onto the Si(001) surface at 100 K, 200 K, and 300 K. By using the MAS scheme, the methanol is allowed to transfer with a small translational energy toward the Si(001) surface and then to interact with the Si dimer(s) on the Si(001) surface. And, this sampling scheme with discrete uniform distribution for methanol placed at the same height above the Si(001) surface enables us to take into account as many reaction pathways as possible and then to evaluate the populations of reaction pathways at different temperatures. Furthermore, the evolutions of dipole moments, bond lengths, and vibrational modes along methanol dissociative adsorption are analyzed by using a Fourier transform of auto-correlation function^{17,18} to understand dynamic behaviors along methanol dissociative adsorption onto the Si(001) surface. Finally, a time-resolved vibrational spectrum constructed by a wavelet transform¹⁹⁻²² provides a better time-resolution at high frequencies than that constructed by short-time Fourier transform, and it clearly illustrates the change of frequency of O-H stretching mode of $\text{CH}_3\text{OH}_{(\text{ads})}$ with time.

Computational Methods

a) AIMD simulations

All static calculations of the structural models of methanol dissociative adsorption onto the Si(001) surface are performed by using SIESTA-3.1 (Spanish Initiative for Electronic Simulations with Thousands of Atoms)²³, a DFT-based code with Troullier-Martins norm-conserving pseudopotentials²⁴. Exchange-correlation energy functional is treated in the Perdew-Burke-Ernzerhof (PBE) of generalized

gradient spin-polarized approximation (GGSA).²⁵ The split valence double-zeta (DZ) basis sets with polarization functions for (1) H ($1s^1$) with a cutoff radius of 1.25 Bohr, (2) C ($2s^22p^2$) with the cutoff radius of 1.49 Bohr, (3) O ($2s^22p^4$) with the cutoff radius of 1.14 Bohr, and (4) Si ($3s^23p^2$) with the cutoff radius of 1.89 Bohr are generated.^{23,26} Following convergence tests of both mesh-cutoff and k points, the calculated lattice parameter of 5.44 Å for bulk silicon is consistent with the experimental value of 5.43 Å.²⁷ Based on this optimized Si crystal structure, the Si surface is represented by a Si(001)-p(2x2) surface and is constructed by a periodically repeated slab of Si atoms with 6 layers in all surface model calculations with a mesh-cutoff of 200 Ry and a $3 \times 3 \times 1$ Monkhorst–Pack mesh.²⁸ The vacuum region for the Si(001)-p(2x2) surface is adopted as 18.0 Å. The bottom of the Si(001)-p(2x2) surface is saturated with hydrogen atoms. The upper 4 layers of Si(001)-p(2x2) surface are allowed to relax, while the bottom 2 layers of Si(001)-p(2x2) surface and the saturated hydrogen atoms are fixed to mimic Si bulk layers.

The DFTMD simulations combined with a MAS scheme are performed by SIESTA in the canonical ensemble (NVT) using Nosé–Hoover thermostat^{31,32} for 10.0 picoseconds (ps) with a time step of 0.5 femtosecond (fs) at 100 K, 200 K, and 300 K, respectively. In this MAS scheme¹⁷, we adopt discrete uniform distribution as the sampling scheme to allow $\text{CH}_3\text{OH}_{(\text{g})}$ at the same height to collide with all possible adsorption sites on the Si (001) surface. Therefore, there are 75 different initial structures of the $\text{CH}_3\text{OH}_{(\text{g})}$ with 3 different orientations placed on the (001) plane of 5×5 grids above 10.0 Å of the Si(001) surface as shown in Figure 1 and 2. Furthermore, the $\text{CH}_3\text{OH}_{(\text{g})}$ is added a small translational energy (4×10^{-5} eV) to direct toward the Si(001) surface at the beginning of each DFTMD calculation and

the optimized structure of $\text{CH}_3\text{OH}_{(g)}$ is selected to be the initial structure for the DFTMD simulations to avoid the influences of the direction of methanol adsorption onto the Si(001) surface. Based on these constraints not only the $\text{CH}_3\text{OH}_{(g)}$ can be guaranteed to transfer toward the Si(001) surface leading to interactions with Si dimers under thermal equilibrium condition but as comprehensive reaction pathways as possible are being taken into account thereby allowing to evaluate the populations of reaction pathways at different temperatures.

b) Time-frequency analysis on the basis of wavelet transform

In our previous study¹⁷ based on short-time Fourier transform of structural coordinate auto-correlation function (STFT-SCAF), it enables us to construct a time-resolved vibrational spectrum – spectrogram – that resolves a complete signal into time-resolved pieces by Fourier transform. In particular, it allows us to discern different types of reaction pathways from time-resolved vibrational spectra and to build the connection between experimental spectra and the variations of vibrational modes along a particular pathway leading to molecular adsorption onto the surface. The STFT-SCAF is given by

$$S^{STFT}(\omega, \tau) = \frac{2\pi\beta\omega^2}{3cV} \int f(t)h(\tau, t)e^{-i\omega t} dt \dots (1)$$

$$f(t) = \langle C(0)_{SC} \cdot C(t)_{SC} \rangle \dots (2)$$

$$h(\tau, t) = \begin{cases} 1 & , \tau \leq t < T + \tau \\ 0 & , \text{otherwise} \end{cases} \dots (3)$$

where $f(t)$ is the SCAF, $C(t)_{SC}$ is time-dependent structural coordinate, τ is the moving time, c is the speed of light, V is the volume, β is Planck constant, ω is the frequency in wavelength, $S^{STFT}(\omega, \tau)$ is a time-resolved spectrum, $h(\tau, t)$ is a window function, and T is the window length whose size determines the resolution of frequency in a time-resolved spectrum.¹⁷ However, due to the fact that the O-H

stretching mode of $\text{CH}_3\text{OH}_{(\text{ads})}$ varies quickly within 1000 fs along this reaction dynamics, the spectrogram constructed by STFT with the window length smaller than 1000 fs and corresponding frequency resolution larger than 66.6 cm^{-1} is not suitable for analyzing the high-frequency shift. It is difficult to resolve the variations of the O-H vibrational mode at the range from 3000 cm^{-1} to 3600 cm^{-1} within 1000 fs.

Following the recent pioneer work by Takao et al.¹⁹⁻²¹, we find that WT is an alternative option to overcome this difficulty in order to improve time resolution in spectrogram. Its original formula is given by

$$S^{WT}(s, \tau) = \int_{-\infty}^{\infty} f(t)w(s, \tau, t)dt \dots (4)$$

$$w(s, \tau, t) = \frac{1}{\pi^{1/4}} e^{-\frac{(t-\tau)^2}{2s^2}} e^{-i\left(\frac{N_c}{s}\right)t} \dots (5)$$

where s is a scaling factor, τ is moving time, $w(s, \tau, t)$ is a Morlet wave composed of a Gaussian window function $e^{-\frac{(t-\tau)^2}{2s^2}}$ multiplied by a plane wave $e^{-i\left(\frac{N_c}{s}\right)t}$, and N_c is the constant. Because the scaling factor s is inversely proportional to the frequency ω , we replace s with ω to reorganize the WT formula in frequency and time domains. The modified WT formula is expressed as

$$S^{WT}(\omega, \tau) = \int_{-\infty}^{\infty} f(t)w^G(\omega, \tau, t)e^{-i\omega t} dt \dots (6)$$

$$w^G(\omega, \tau, t) = \frac{1}{\pi^{1/4}} e^{-\frac{\omega^2(t-\tau)^2}{2N_c^2}} \dots (7)$$

where ω is frequency in cm^{-1} , τ is moving time, $w^G(\omega, \tau, t)$ is a Gaussian window function, and the constant N_c is relevant to the full width at half maximum (FWHM) of a Gaussian window function. Both Eq. (1) of STFT and Eq. (6) of the WT are quite similar, except for different window functions that are being used. It is noticeable that the window function in WT has one more parameter ω to be

considered. Consequently, the shape (or length) of the window function in WT will change with ω , whereas that in STFT is independent of ω . For instance, in Figure 3, two wavelets with different frequency, one is 8 and another is 16, are shown to illustrate that the window length would become smaller as ω becomes larger. In other words, the smaller window length is generated to improve a spectrogram in the time domain as the higher frequency signal is transformed.

To elaborate this WT a bit further we take combinations of sine waves expressed as below and shown in Figure 4 as an example to illustrate the better time resolution of a spectrogram by using WT.

$$f(t) = \sin(36t) e^{-\left(\frac{t-n/6}{c}\right)^2} + \sin(40t) e^{-\left(\frac{t-3n/6}{c}\right)^2} + \sin(32t) e^{-\left(\frac{t-5n/6}{c}\right)^2} \dots (8)$$

where total time steps n is 1000 fs and the constant c is 40. The Figure 5 shows that there are three different peaks in frequency domain, i.e. 2958, 3333, and 3708 cm^{-1} . But this spectrum by FT doesn't have time resolution to show at what time intervals these frequencies appear. Therefore, we use WT to construct the spectrogram as shown in Figure 6 to illustrate that three peaks are resolved simultaneously in both time and frequency domains.

According to the definition of the FWHM of Gaussian function in the Eq. (9), the FWHM of a Gaussian window function in WT at frequency of 2958 cm^{-1} is evaluated to be about 365 fs.

$$\text{FWHM}_{\text{Gauss}} = 2\sqrt{2\ln 2} \left(\frac{N_c}{\omega}\right)^2 \cong 2.35482 \left(\frac{N_c}{\omega}\right)^2 \dots (9)$$

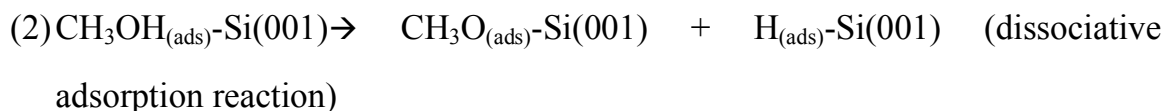
where N_c is 15. It clearly demonstrates that the window length is small enough to resolve these sine waves within 1000 fs. Based on these analyses we are convinced that the WT is an appropriate approach to allow us to investigate the variation of the O-H stretching mode when methanol adsorbs onto the Si(001) surface.

Results and discussion

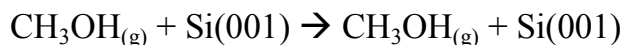
a) Reaction pathways of methanol adsorption onto Si(001) surface

The methanol adsorption onto the Si(001)-p(2x2) surface is simulated by DFTMD in association with a MAS scheme at 100 K, 200 K, and 300 K, respectively. According to the temperature-controlled trajectories of the Si-O bond length during DFTMD simulations, as shown in Figure 7, two types of reaction pathways are categorized as follows.

a. Dissociative adsorption:



b. Repelling reaction:



The dissociative adsorption in which the $\text{CH}_3\text{OH}_{(g)}$ firstly is adsorbed on the buckled-down Si atom and then the O-H bond of the $\text{CH}_3\text{OH}_{(ads)}$ is dissociated to form both $\text{CH}_3\text{O}_{(ads)}$ and $\text{H}_{(ads)}$ fragments adsorbed on the Si dimer. It is a two-step reaction process that involves (1) direct adsorption and (2) dissociative adsorption reaction.

In direct adsorption, when the $\text{CH}_3\text{OH}_{(g)}$ is translated to the Si(001) surface, the lone pair orbital of the O atom of the $\text{CH}_3\text{OH}_{(g)}$ is attracted by the dangling bond of

the Si dimer(s), and the distance between Si atom and O atom is getting shorter and reaches a minimum at approximately 2.3 ps as shown in Figure 7 and Figure 8. The average total energy of the $\text{CH}_3\text{OH}_{(\text{ads})}$ at stage 2 as shown in Figure 9 is about 0.82 eV lower than that of the $\text{CH}_3\text{OH}_{(\text{g})}$ at stage 1. Subsequent to the forming of Si-O bond, the valence electrons on the O atom are shared with the buckled-down Si atom and the average Si-O bond length from 2.5 ps to 5.5 ps is estimated about 2.113 Å. It leads to the fact that both O-H and C-O bond lengths become longer. Furthermore, due to the weakening of C-O bond, the interactions between the C atom and the H atoms are indirectly strengthened and hence the C-H bond lengths become shorter as listed in Table 1. The adsorbed structure of the $\text{CH}_3\text{OH}_{(\text{ads})}$ in this direct adsorption is reasonably consistent with those models proposed by static calculations^{11,12} and experimental IR spectra at 100 K⁶.

Following the direct adsorption, the $\text{H}_{(\text{ads})}$ atom of the O-H bond of $\text{CH}_3\text{OH}_{(\text{ads})}$ points to the buckled-up Si atom of the adjacent dimer(s), $\text{Si}_{\text{adj-up}}$, at most of the time because it is easily attracted by the Si dangling bond. Due to thermal effect and the O-H bond weakening by substrate, the dissociative adsorption reaction occurs only at 300 K through DFTMD simulations within 10.0 ps. This reaction involves the dissociation of the O-H bond to form $\text{CH}_3\text{O}_{(\text{ads})}$ and $\text{H}_{(\text{ads})}$ fragments adsorbed on the Si dimer as shown in Figure 8. According to our static calculations in Table 2, the total energy of the O-H bond pointing to the $\text{Si}_{\text{adj-up}}$ atom is slightly lower (about 0.03 eV) than the O-H bond pointing to the same buckled-up Si atom ($\text{Si}_{\text{same-up}}$). It implies that the probability of the O-H bond pointing to the $\text{Si}_{\text{adj-up}}$ atom is larger than that of the O-H bond pointing to the $\text{Si}_{\text{same-up}}$ atom. Therefore, the probability of the O-H bond cleavage through the $\text{Si}_{\text{adj-up}}$ atom is higher than that of the O-H bond cleavage through the $\text{Si}_{\text{same-up}}$ atom. Then, after the O-H bond cleavage, the valence electrons of the O

atom of $\text{CH}_3\text{OH}_{(\text{ads})}$ are redistributed to the neighboring Si-O and C-O bonds. The average Si-O and C-O bond lengths are shortened to about 1.697 and 1.438 Å between 6.0 ps and 10.0 ps. At the same time, because of the strengthening of C-O bond, the C-H bonds are indirectly weakening and their bond lengths are elongated to about 1.103 Å. Regarding the average total energy at stage 3 as shown in Figure 9, it is about 1.62 eV more stable than that of $\text{CH}_3\text{OH}_{(\text{ads})}$ at stage 2. However, according to our calculated results as listed in Table 3, there is no any dissociative reaction of the C-O bond to form the CH_3 and OH fragments adsorbed on the Si(001) surface. This is because the activation energy of the C-O bond cleavage in static calculations is estimated about 1.2 eV¹² and the $\text{CH}_3_{(\text{ads})}$ species is formed only at substrate temperature 600 K³. In comparison with the higher activation energy of the C-O bond cleavage, the low activation energy of the O-H bond cleavage about 0.2 eV is much easier to overcome.^{11,12} In addition, Miotto et al. showed that the C-H bond cleavage of $\text{CH}_3\text{OH}_{(\text{ads})}$ has the high activation energy about 0.8 eV (79 kJ/mol).¹⁵ Based on static calculations, we find that the difference of total energies between optimized structures, i.e. $\text{CH}_2\text{OH}_{(\text{ads})} + \text{H}_{(\text{ads})}$ and $\text{CH}_3\text{O}_{(\text{ads})} + \text{H}_{(\text{ads})}$, is about 1.0 eV as shown in Table 4 and $\text{CH}_3\text{O}_{(\text{ads})} + \text{H}_{(\text{ads})}$ is the most stable structure. This static comparison indicates that the our final structure, i.e. $\text{CH}_3\text{O}_{(\text{ads})} + \text{H}_{(\text{ads})}$, is the best option for methanol dissociative adsorption on Si(001) surface. Therefore, the methanol dissociative adsorption via the O-H bond cleavage in our DFTMD simulations is in good agreement with experimental and theoretical results.^{3,6,12,15}

Regarding the repelling reaction the H atom of $\text{CH}_3\text{OH}_{(\text{g})}$ will directly interact with the Si dimer rather than the O atom of $\text{CH}_3\text{OH}_{(\text{g})}$. Consequently, the $\text{CH}_3\text{OH}_{(\text{g})}$ is repelled by the Si atoms of Si dimer to leave the Si(001) surface. Based on the trajectory of the Si-O bond length, the distance between both Si atom and O atom is

always larger than 3.0 angstroms. Obviously, it shows that $\text{CH}_3\text{OH}_{(\text{g})}$ does not bond with any Si atoms. From the viewpoint of dynamic behaviors, the $\text{CH}_3\text{OH}_{(\text{g})}$ firstly approaches the Si(001) surface in such a way that (1) the O-H bond of the $\text{CH}_3\text{OH}_{(\text{g})}$ (or its C-H bond) is perpendicular to the Si(100) surface and (2) its H atom is attached to a Si atom, then the $\text{CH}_3\text{OH}_{(\text{g})}$ will be repelled by the Si atom due to the repulsion between H atom and Si atom along z-axis. As a result, the $\text{CH}_3\text{OH}_{(\text{g})}$ escapes from the Si(001) surface during repelling reaction. This is an ineffective collision, which is similar to previous study of the ethylene adsorption on the same surface¹⁷. However, as long as the angle between the O-H bond and the Si(001) surface is not perpendicular, the $\text{CH}_3\text{OH}_{(\text{g})}$ is possible to change its structural orientation thereby allowing the lone pair orbital of its O atom to be attracted by the dangling bond of the Si dimer. It results in the attraction between the O atom and the Si atom to form the Si-O bond. This explains that the main reaction pathway goes through the direct adsorption.

b) Calculated infrared spectra of methanol dissociative adsorption onto Si(001) surface

Having discussed the dissociative adsorption and the variations of bond lengths of the CH_3OH at different stages, it is essential to establish the connection between the dissociative adsorption and corresponding experimental IR spectra. Therefore, we calculate the vibrational modes of CH_3OH at three stages, that is, $\text{CH}_3\text{OH}_{(\text{g})}$, $\text{CH}_3\text{OH}_{(\text{ads})}$, and $\text{CH}_3\text{O}_{(\text{ads})} + \text{H}_{(\text{ads})}$, by using a Fourier transform of the dipole moment auto-correlation function scheme¹⁸ and then investigate that the IR active peaks of the CH_3OH evolve along methanol dissociative adsorption onto the Si(001) surface. In the following paragraph, the variations of different vibrational modes are

described in detail.

As shown in Figure 10 and table 5, before the $\text{CH}_3\text{OH}_{(\text{ads})}$ is adsorbed on the Si(001) surface, the IR peaks of the C-O stretching mode, the CH_3 rocking mode, and the C-H stretching modes are 1001 cm^{-1} , 1163 cm^{-1} , 2922 cm^{-1} , and 3057 cm^{-1} , respectively, which is in good agreement with the experimental IR spectrum³³. When the $\text{CH}_3\text{OH}_{(\text{ads})}$ is adsorbed on the buckled-down Si atom, the Si-Si stretching mode is red-shifted from 667 cm^{-1} to 567 cm^{-1} because of the Si-Si bond weakening. At the same time, the C-O stretching mode of the $\text{CH}_3\text{OH}_{(\text{ads})}$ shows the red-shift from 1001 to 912 cm^{-1} due to the elongation of its bond length, and the C-H stretching modes of $\text{CH}_3\text{OH}_{(\text{ads})}$ are blue-shifted due to the strengthening of the C-H bonds as shown in Figure 10-b. Then, after the O-H bond of the $\text{CH}_3\text{OH}_{(\text{ads})}$ attracted by the $\text{Si}_{\text{adj-up}}$ atom is dissociated, both C-O and Si-O bond lengths of the $\text{CH}_3\text{O}_{(\text{ads})}$ become shorter. It leads to the blue-shift of the C-O stretching mode at 1034 cm^{-1} and the appearance of the Si-O stretching modes at 684 cm^{-1} . In contrast, due to the elongation of the C-H bond lengths, the symmetrical and asymmetrical C-H stretching modes shows the red-shift to 2877 cm^{-1} and 2935 cm^{-1} , respectively. Furthermore, because the dissociated H atom is adsorbed on the $\text{Si}_{\text{adj-up}}$ atom, the peak of the Si-H stretching mode appears at 2068 cm^{-1} as shown in Figure 10-c. These calculated results along this reaction pathway reasonably agree with the experimental IR spectra⁶.

c) The time-resolved spectra of the O-H stretching mode by wavelet transform

Since $\text{CH}_3\text{OH}_{(\text{ads})}$ was initially adsorbed on the buckled-down Si atom at stage 1, the frequencies of its O-H stretching mode are distributed widely, ranging from 3400 to 3600 cm^{-1} as shown in Figure 10-b. At stage 2, the variations of adsorbed

structures along the dissociative adsorption pathway can't be identified from just one calculated IR spectrum without temporal resolution. In order to understand what factors influence the frequency shift of the O-H stretching mode leading to the wide distribution within calculated IR spectrum at stage 2, we use the WT-SCAF to detect the trajectory of the O-H bond as shown in Figure 11 and then to construct corresponding time-resolved vibrational spectrum before the cleavage of the O-H bond.

Prior to adsorption of $\text{CH}_3\text{OH}_{(\text{ads})}$ onto Si(001) surface, the O-H stretching mode of $\text{CH}_3\text{OH}_{(\text{g})}$ from 0.0 ps to 2.0 ps is observed at about 3686 cm^{-1} as shown in Figure 12, which corresponds to the O-H vibrational mode of $\text{CH}_3\text{OH}_{(\text{g})}$ at 3681 cm^{-1} in experimental IR spectrum³³. Then, after the lone pair orbital of the O atom bonds to the buckled-down Si atom at about 3.0 ps, 3.6~4.0 ps, and 5.5 ps, the O-H bond of the $\text{CH}_3\text{OH}_{(\text{ads})}$ is weakened and corresponding O-H stretching mode is red-shifted to $3500\sim 3600\text{ cm}^{-1}$, which is consistent with 3589 cm^{-1} calculated by the normal mode calculation in slab model¹⁵. In the meantime, the distances between the H atom (H_O) of the O-H bond and all of buckled-up Si atoms ($\text{H}_\text{O}\cdots\text{Si}_{\text{up}}$) are larger than 2.6 \AA . It implies that the interactions between this H_O atom and the buckled-up Si atoms are weak. Therefore, this frequency shift of the O-H stretching mode of $\text{CH}_3\text{OH}_{(\text{ads})}$ is mainly caused by the Si-O bond to weaken the O-H bond.

However, the O-H bond of $\text{CH}_3\text{OH}_{(\text{ads})}$ is able to rotate around the Si dimer and its H_O atom is possible to point to the buckled-up Si atoms. First, we found that when this H_O atom points to the $\text{Si}_{\text{adj-up}}$ atom at about 2.4~2.8 ps and 3.2~3.5 ps, the O-H stretching mode of $\text{CH}_3\text{OH}_{(\text{g})}$ at 3686 cm^{-1} is red-shifted to a lower frequency ranging from 3000 to 3300 cm^{-1} as shown in Figure 12. This is due to the fact that

the H_O atom is attracted by the dangling bond of the Si_B atom and the $H_O \cdots Si_B$ distance is shorter than 2.6 Å. Owing to this $H_O \cdots Si_B$ attraction, then, the O-H bond is weakened further and the O-H bond length is stretched more than its average length of 0.994 Å. As a result, its O-H stretching mode is lower than 3500 cm^{-1} . Additionally, after the O-H bond of $CH_3OH_{(ads)}$ rotates to opposite direction at 4.2~4.5 ps as shown in Figure 12, its H_O atom points to the Si_A atom. The H_O atom is also attracted by the dangling bond of the Si_A atom and hence its O-H bond is stretched about 1.12 Å as shown in Figure 11. Consequently, its O-H stretching mode appears at about 3250 cm^{-1} . However, at about 5.1 ps, this H_O atom temporarily points to the Si_C atom at the same dimer, and the $H_O \cdots Si_C$ distance is close to 2.4 angstroms. Similarly, due to the $H_O \cdots Si_C$ attraction, the O-H bond length is longer and its frequency is slightly red-shifted to about 3400 cm^{-1} .

According to these analyses, two main factors causing frequency shifts of the O-H stretching mode from 3686 cm^{-1} to $3000\sim 3600\text{ cm}^{-1}$ are illustrated as follows. First, the frequency of O-H stretching mode shifted to $3500\sim 3600\text{ cm}^{-1}$ is attributed to the Si-O bonding through the interaction of the O atom of $CH_3OH_{(ads)}$ with buckled-down Si atom of the Si dimer to weaken the O-H bond. Second, when the H_O atom points to one of three buckled-up Si atoms, the attraction force between the H_O atom and the buckled-up Si atom can cause the O-H bond to stretch further. It turns out that the O-H stretching mode is shifted to lower frequency and appears at the range from 3000 cm^{-1} to 3400 cm^{-1} . In addition, due to the thermal effect, the O-H bond which points to the buckled-up Si atom rotates with swing motion back and forth on the surface plane. Thus, the frequency of the O-H stretching mode of $CH_3OH_{(ads)}$ changes with different extent of interactions between the Si atom and the H_O atom. This leads to a wide distribution of the O-H stretching mode at about

3000~3400 cm^{-1} in IR spectrum. It is also believed that this similar dynamic motion of the O-H bond causes the O-H stretching mode of ethanol adsorbed on the Si(001) surface to give rise to the experimental IR broad peak around 3267 cm^{-1} at 135 K⁷.

d) The effect of temperature for methanol dissociative adsorption

As substrate temperature increases up to 150 K, the vibrational spectra show that the peak of the Si-H stretching mode appears in 2091 cm^{-1} . It implies that the O-H bond cleavage of the $\text{CH}_3\text{OH}_{(\text{ads})}$ is governed by the thermal effect to form both products of $\text{CH}_3\text{O}_{(\text{ads})}$ and $\text{H}_{(\text{ads})}$ on the Si dimer. In order to investigate how temperature influences the reaction process of the dissociative adsorption, we analyzed (1) distributions of the angle between the O-H bond and the Si dimer and (2) distributions of the O-H bond length at 100 K, 200 K, and 300 K to understand the dynamic behaviors of the O-H bond at different temperatures.

After the $\text{CH}_3\text{OH}_{(\text{ads})}$ is adsorbed on the Si(001) surface, its O-H bond could rotate randomly on the buckled-down Si atom. According to the distributions of the angle between the O-H bond and the Si-Si dimer in the Si(001) surface at 100 K, 200 K, and 300 K as shown in Figure 13, it clearly points out that the H_O atom is easily to be attracted by the $\text{Si}_{\text{adj-up}}$ atom rather than the $\text{Si}_{\text{same-up}}$ atom. As temperature increases, the rotational angle of the O-H bond is getting larger. Thus, the distribution of the angle at high temperature is broader than that at low temperature. Although the O-H bond is prone to point toward the $\text{Si}_{\text{adj-up}}$ atom at low temperature due to the weak attraction force between the H_O atom and the $\text{Si}_{\text{adj-up}}$ atom, it is hardly to trigger the O-H bond cleavage at low temperature according to the populations of reaction pathways as shown in Table 3. On the contrary, the less

probability of the O-H bond pointing to the $\text{Si}_{\text{adj-up}}$ atom at high temperature than that at low temperature does prompt dissociative reaction to occur easily. It implies that the weak attraction between the H_O atom and the $\text{Si}_{\text{adj-up}}$ atom is not enough to break the O-H bond leading to the formation of the Si-H bond. Apparently, this attraction is not the main factor for the O-H bond cleavage.

In Figure 14, it shows the distributions of the O-H bond length of $\text{CH}_3\text{OH}_{(\text{ads})}$ and corresponding standard deviations at 100 K, 200 K, and 300 K. The distribution of the O-H bond length at high temperature is broader than that at low temperature. Also, its standard deviation is getting larger as temperature rises. It means that when the O-H bond length is stretched longer at high temperature, its H_O atom will be closer to the $\text{Si}_{\text{adj-up}}$ atom. As a result, this H_O atom is easier to be attracted by the $\text{Si}_{\text{adj-up}}$ atom. At the same time, the O-H bond becomes weaker and the Si-O bond becomes shorter. Consequently, it leads to the cleavage of the O-H bond and the formation of the new $\text{Si}_{\text{adj-up}}\text{-H}$ bond. Therefore, in addition to the attraction between the H_O atom and the $\text{Si}_{\text{adj-up}}$ atom, the elongation of the O-H bond governed by thermal effect dictates the increasing probability of the O-H bond cleavage in the methanol dissociative adsorption.

In our DFTMD calculations, one of two Si dimers is occupied by a $\text{CH}_3\text{OH}_{(\text{ads})}$ (about 0.5 monolayer (ML)) and the O-H bond of the $\text{CH}_3\text{OH}_{(\text{ads})}$ could rotate with swing motion back and forth randomly on the surface. However, in the case of the high coverage (i.e. 1.0 ML), two methanols will occupy two neighboring Si dimers at the same time. The O-H bonds of these two $\text{CH}_3\text{OH}_{(\text{ads})}$ could have repulsions between their both H_O atoms because their O-H bonds could be too close to rotate freely on the Si(001) surface. Then, the rotational angles of both O-H bonds on the Si(001) surface

could be constrained as shown in Figure 15. Therefore, most of the time, these two O-H bonds could point to the buckled-up Si atoms. Both O-H bonds will be easier to be attracted by the $\text{Si}_{\text{adj-up}}$ atoms. It means that the high coverage of $\text{CH}_3\text{OH}_{(\text{ads})}$ on the Si(001) surface could increase the possibility of the O-H bond cleavage to form $\text{CH}_3\text{O}_{(\text{ads})}$ and $\text{H}_{(\text{ads})}$. Consequently, it will increase the reaction rate of methanol dissociative adsorption on the Si(001) surface. From this viewpoint, we expect that one can observe different dynamic behaviors of methanol dissociative adsorption with different coverage, such as 0.5 ML and 1.0 ML. In addition, at the higher temperature it is easier to trigger the elongation of the O-H bond and then to make the $\text{Si}_{\text{adj-up}}$ atom attracts the H_O atom. Therefore, temperature is the important factor to speed up the O-H bond cleavage. We also expect that methanol dissociative adsorption on Si(001) surface at higher coverage will occur easily within 10 ps, especially at higher temperature. Based on this study, presently, we are performing the simulations of methanol dissociative adsorption on different types of a Si wafer surface, that is, Si(111) and Si(110), to differentiate reaction processes from them and to discuss about the relation between coverage and temperature effect.

Conclusion

The thermally-induced reaction and vibration dynamics of methanol dissociative adsorption onto Si(001) surface at 100 K, 200 K, and 300 K have been investigated by combing DFTMD simulations with a MAS scheme and a wavelet transform. During the methanol dissociative adsorption, the $\text{CH}_3\text{OH}_{(\text{ads})}$ is first adsorbed on the Si(001) surface and its O-H bond length is stretched due to the Si-O bonding and the attraction between the H_O atom and the buckled-up Si atoms. After the O-H bond is weakened, the O-H stretching mode of $\text{CH}_3\text{OH}_{(\text{g})}$ at 3686 cm^{-1} is red-shifted to lower

frequency as wider range from 3000 to 3400 cm^{-1} in time-resolved spectra constructed by WT-SCAF, which is consistent with the broad peak around 3267 cm^{-1} observed experimentally.⁷ At high temperature, the O-H bond length is stretched further leading to the larger attraction between its H_O atom and the buckled-up Si atom. Therefore, the O-H bond is dissociated to form Si-H bond and the CH₃O_(ads) species on the Si(001) surface only at 300 K. Subsequent to the O-H bond cleavage, the Si-H stretching mode of 2068 cm^{-1} appears in the calculated IR spectrum, which is also in good agreement with the experimental Si-H peak at 2091 cm^{-1} .

Acknowledgements

The authors would like to thank the National Science Council in Taiwan (Grant nos. NSC 102-2113-M-032-004) for financial support and Tamkang University in Taiwan for the use of computational facilities.

References

- 1 R. C. Henderson, *J. Electrochem. Soc.* 1972, **119**, 772-775.
- 2 F. Shimura, "Semiconductor Silicon Crystal Technology (Academic Press, San Diego)", Appendix XII, 1989.
- 3 J. A. Glass, E. A. Wovchko, J. T. Yates, Jr., *Surf. Sci.* 1995, **338**, 125-137.
- 4 J. E. Crowell, L. L. Tedder, H. C. Cho, F. M. Cascarano, *J. Vac. Sci. Technol. A* 1990, **8**, 1864-1870.
- 5 L. L. Tedder, G. Lu, J. E. Crowell, *J. Appl. Phys.* 1991, **69**, 7037-7049.
- 6 W. Ehrley, R. Butz, S. Mantl, *Surf. Sci.* 1991, **248**, 193-200.
- 7 J. Eng, Jr., K. Raghavachari, L. M. Struck, Y. J. Chabal, B. E. Bent, G. W. Flynn, S. B. Chrisman, E. E. Chaban, G. P. Williams, K. Radermacher, S. Mantl, *J. Chem. Phys.* 1997, **106**,

9889-9898.

- 8 M. P. Casaletto, R. Zanoni, M. Carbone, M. N. Piancastelli, L. Aballe, K. Weiss, K. Horn, *Surf. Sci.* 2002, **505**, 251-259.
- 9 M. P. Casaletto, R. Zanoni, M. Carbone, M. N. Piancastelli, L. Aballe, K. Weiss, K. Horn, *Surf. Sci.* 2000, **447**, 237-244.
- 10 L. Zhang, A. J. Carman, S. M. Casey, *J. Phys. Chem. B* 2003, **107**, 8424-8432.
- 11 X. Lu, Q. Zhang, M. C. Lin, *Phys. Chem. Chem. Phys.* 2001, **3**, 2156-2161.
- 12 T. Kato, S. Y. Kang, X. Xu, T. Yamabe, *J. Phys. Chem. B* 2001, **105**, 10340-10347.
- 13 Y. Wang, G. S. Hwang, *J. Chem. Phys.* 2005, **122**, 164702-164706.
- 14 M. Carbone, K. Larsson, *J. Phys.: Condens. Matter* 2005, **17**, 1289-1300.
- 15 R. Miotto, G. P. Srivastava, A. C. Ferraz, *Surf. Sci.* 2005, **575**, 287-299.
- 16 T. H. Lin, B. Y. Lin, T. Hao, H. Y. Chien, J. H. Wang, W. H. Hung, *J. Phys. Chem. C* 2013, **117**, 2760-2768.
- 17 Y. T. Lee, J. S. Lin, *J. Comput. Chem.* 2013, **34**, 2697-2706.
- 18 J. S. Lin, S. Y. Lu, P. J. Tseng, W. C. Chou, *J. Comput. Chem.* 2012, **33**, 1274-1283.
- 19 A. Rahaman, R. A. Wheeler, *J. Chem. Theory Comput.* 2005, **1**, 769-771.
- 20 T. Otsuka, H. Nakai, *J. Comput. Chem.* 2007, **28**, 1137-1144.
- 21 M. Pagliai, F. Muniz-Miranda, G. Cardini, R. Righini, S. Vincenzo, *J. Mol. Struct.* 2011, **993**, 438-442.
- 22 R. H. Landau, M. J. Páez, C. C. Bordeiano, *A survey of computational physics*, Princeton University Press, 2008.
- 23 J. M. Soler, E. Artacho, J. D. Gale, A. Garcia, J. Junquera, P. Ordejón, D. Sánchez-Portal, *J. Phys. Condens. Matter* 2002, **14**, 2745-2779.
- 24 N. Troullier, J. L. Martins, *Phys. Rev. B* 1991, **43**, 1993-2006.
- 25 J. P. Perdew, K. Burke, M. Ernzerhof, *Phys. Rev. Lett.* 1996, **77**, 3865-3868.
- 26 J. Junquera, Ó. Paz, D. Sánchez-Portal, E. Artacho, *Phys. Rev. B* 2001, **64**, 235111-235119.
- 27 C. Kittel, *Introduction to Solid State Physics*, 8th ed.; John Wiley & Sons, 2005; Chapter 1,

pp 20.

- 28 H. J. Monkhorst, J. D. Pack, *Phys. Rev. B* 1976, **13**, 5188-5192.
- 29 A. Ramstad, G. Brocks, P. J. Kelly, *Phys. Rev. B* 1995, **51**, 14504-14523.
- 30 N. Roberts, R. J. Needs, *Surf. Sci.* 1990, **236**, 112-121.
- 31 S. Nosé, *J. Chem. Phys.* 1984, **81**, 511-519.
- 32 S. Nosé, *Mol. Phys.* 1984, **52**, 255-268.
- 33 NIST Chemistry Webbook, NIST Standard Reference Database Number 69,
<http://webbook.nist.gov/chemistry/> (accessed Feb. 9, 2015).

Figure Captions

Figure 1. The structural model of the $\text{CH}_3\text{OH}_{(\text{g})}$ above 10 \AA of the $\text{Si}(001)$ surface in the beginning of DFTMD simulations is shown from the side view. The orange dash-line shows that the initial position of $\text{CH}_3\text{OH}_{(\text{g})}$ is placed on the (001) plane. The red arrow indicates the direction of the motion of $\text{CH}_3\text{OH}_{(\text{g})}$ with a translational energy of $4 \times 10^{-5} \text{ eV}$.

Figure 2. Three types (a), (b), and (c) of initial structures of $\text{CH}_3\text{OH}_{(\text{g})}$ above 10.0 \AA of the $\text{Si}(001)$ surface.

Figure 3. Two wavelet waves in blue line show different window lengths which depends on the scale factor s or frequency ω . The Gaussian window function is shown in green line.

Figure 4. According to the equation (8), the signal is composed of sine waves in 1.0 ps .

Figure 5. Three peaks of 2958 , 3333 , and 3708 cm^{-1} are shown in the power spectrum of sine waves by using Fourier transform.

Figure 6. The time-resolved spectrum of sine waves shows three peaks at different time. The first peak at 166 fs is 3333 cm^{-1} , the second one at 500 fs is 3708 cm^{-1} , and the last one at 833 fs is 2958 cm^{-1} .

Figure 7. The trajectories of the Si-O bond length along the dissociative adsorption and repelling reaction are shown. Both red and blue arrows indicate the time at

which the $\text{CH}_3\text{OH}_{(\text{g})}$ is attached to the surface.

Figure 8. The structural models illustrate that (1) the $\text{CH}_3\text{OH}_{(\text{ads})}$ is translated toward the Si(001) surface at stage 1, (2) the O atom of the $\text{CH}_3\text{OH}_{(\text{ads})}$ bonds with the buckled-down Si atom at stage 2, and (3) both $\text{CH}_3\text{O}_{(\text{ads})}$ and $\text{H}_{(\text{ads})}$ species are adsorbed on the Si(001) surface subsequent to the O-H bond cleavage.

Figure 9. The total energy trajectory subtracted by that at the first step of the DFTMD simulation along the dissociative adsorption.

Figure 10. The calculated IR spectra at 3 stages, i.e. $\text{CH}_3\text{OH}_{(\text{g})}$, $\text{CH}_3\text{OH}_{(\text{ads})}$, and $\text{CH}_3\text{O}_{(\text{ads})} + \text{H}_{(\text{ads})}$ are shown, respectively. Based on the O-H dipole moment at stage 1 and stage 2, the IR peaks of the O-H stretching mode are shown in the both insets.

Figure 11. The trajectory of the O-H bond length along the dissociative adsorption from 0.0 ps to 6.0 ps is shown.

Figure 12. The distances between the H_O atom and the buckled-up Si atoms are shown in the middle figure, and the time-resolved spectrum constructed by WT-SCAF is shown in the bottom figure.

Figure 13. The distributions of the angle between the Si dimer and the O-H bond at 100 K (green line), 200 K (blue line), and 300 K (red line) are shown. In the structural figure, the black and blue arrows mean the vectors of the Si dimer and the O-H bond, respectively.

Figure 14. The distributions of the O-H bond length at 100 K (green line), 200 K (blue line), and 300 K (red line) are shown. The right inset indicates that the standard deviations of the O-H bond length at these temperatures are 0.0152, 0.0160, and 0.0165 Å, respectively.

Figure 15. The structural model (top view) of two methanols adsorbed on the Si(001) surface. The dash-line with yellow color could be the constrained rotational range due to the repulsions between H_O atoms, while the dash-line with blue color could be the allowed rotational range of the O-H bond of the methanol adsorbed on the Si(001) surface.

Table Captions

Table 1. In the dissociative adsorption, the various bond lengths at three stages are listed, i.e. $\text{CH}_3\text{OH}_{(\text{g})}$, $\text{CH}_3\text{OH}_{(\text{ads})}$, and $\text{CH}_3\text{O}_{(\text{ads})}+\text{H}_{(\text{ads})}$.

Table 2: Total energies of optimized $\text{CH}_3\text{OH}_{(\text{ads})}$ on the Si(001) surface.

Table 3. The counts of two reaction pathways and corresponding populations at 100 K, 200 K, and 300 K are listed. Total number of the DFTMD simulations at each temperature is 75.

Table 4: Total energies of $\text{CH}_3\text{O}_{(\text{ads})}+\text{H}_{(\text{ads})}$ and $\text{CH}_2\text{OH}_{(\text{ads})}+\text{H}_{(\text{ads})}$ on the Si(001) surface.

Table 5. The calculated IR spectra of methanol dissociative adsorption, corresponding experimental IR spectra, and normal mode calculations are listed.

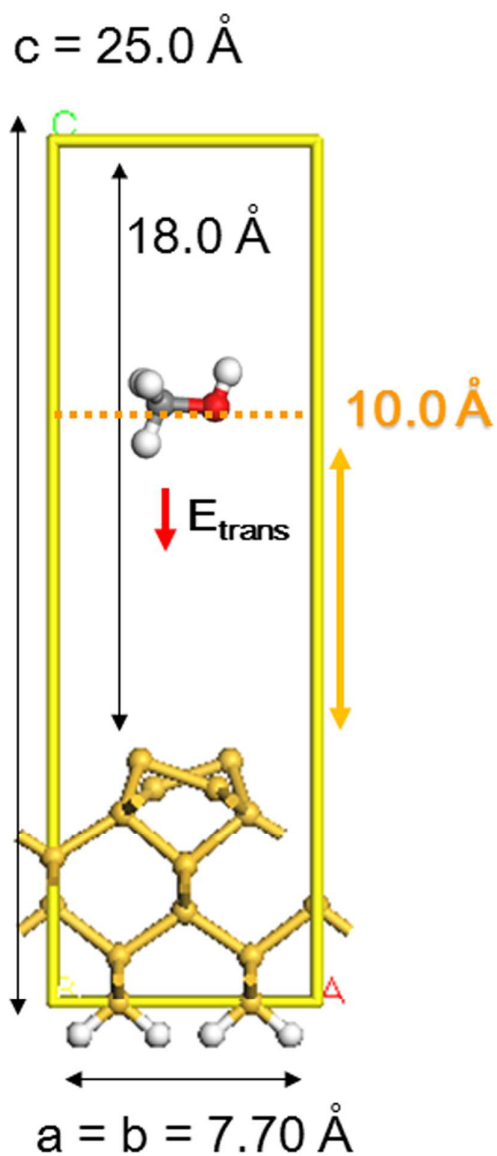


Figure 1. The structural model of the $\text{CH}_3\text{OH}_{(g)}$ above 10 \AA of the $\text{Si}(001)$ surface in the beginning of DFTMD simulations is shown from the side view. The orange dash-line shows that the initial position of $\text{CH}_3\text{OH}_{(g)}$ is placed on the (001) plane. The red arrow indicates the direction of the motion of $\text{CH}_3\text{OH}_{(g)}$ with a translational energy of $4 \times 10^{-5} \text{ eV}$.

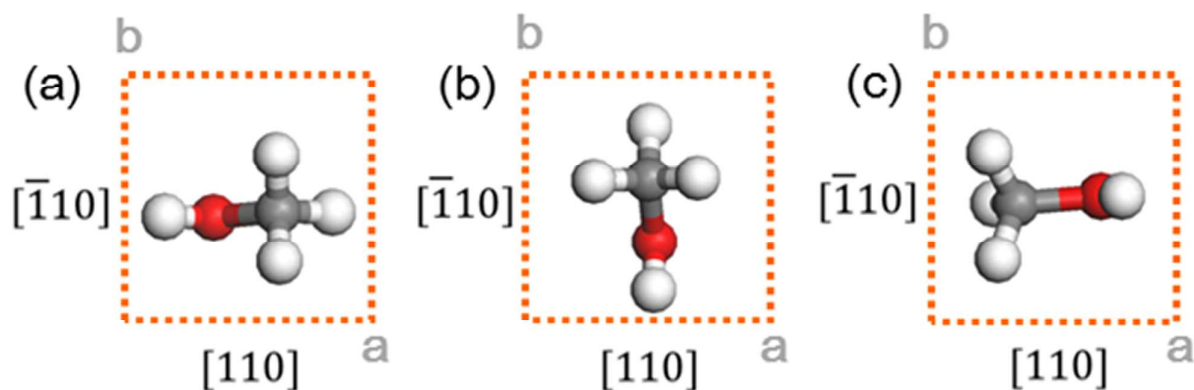


Figure 2. Three types (a), (b), and (c) of initial structures of CH₃OH_(g) above 10.0 Å of the Si(001) surface.

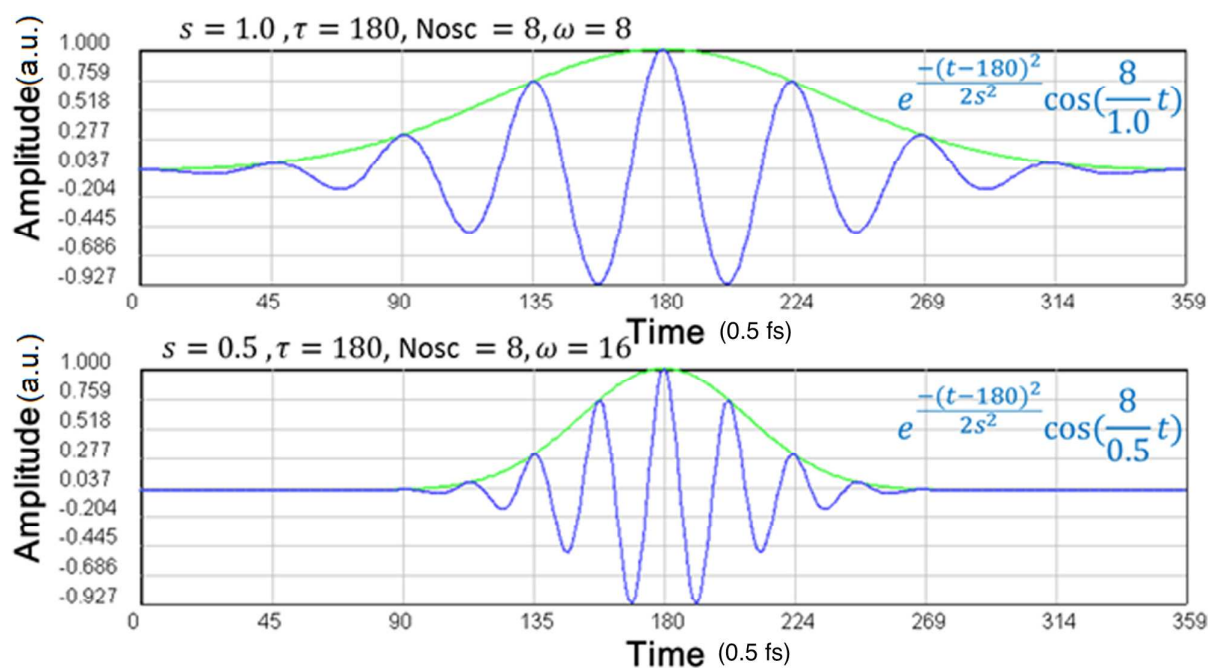


Figure 3. Two wavelet waves in blue line show different window lengths which depends on the scale factor s or frequency ω . The Gaussian window function is shown in green line.

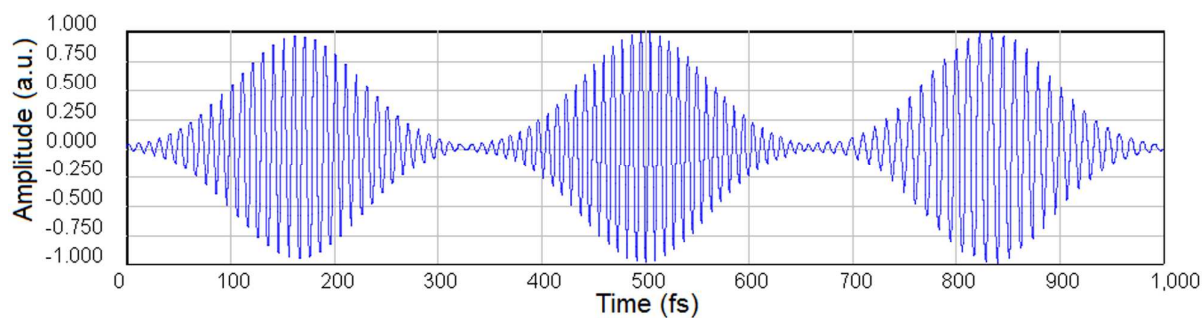


Figure 4. According to the equation (8), the signal is composed of sine waves in 1.0 ps.

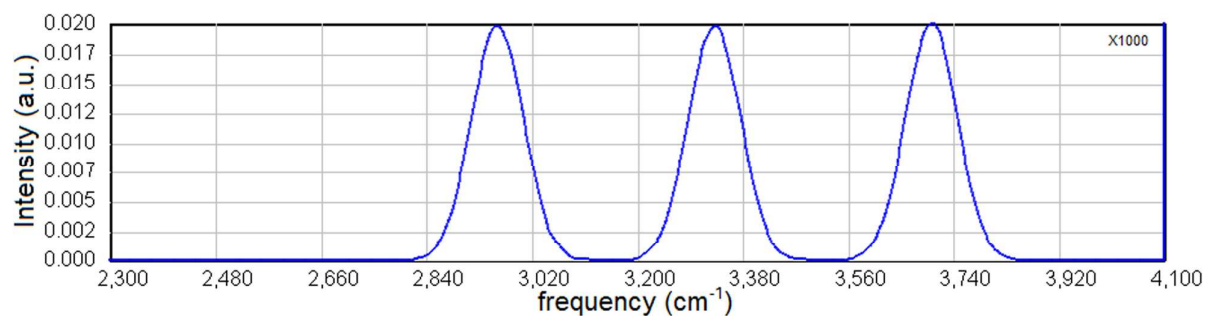


Figure 5. Three peaks of 2958, 3333, and 3708 cm^{-1} are shown in the power spectrum of sine waves by using Fourier transform.

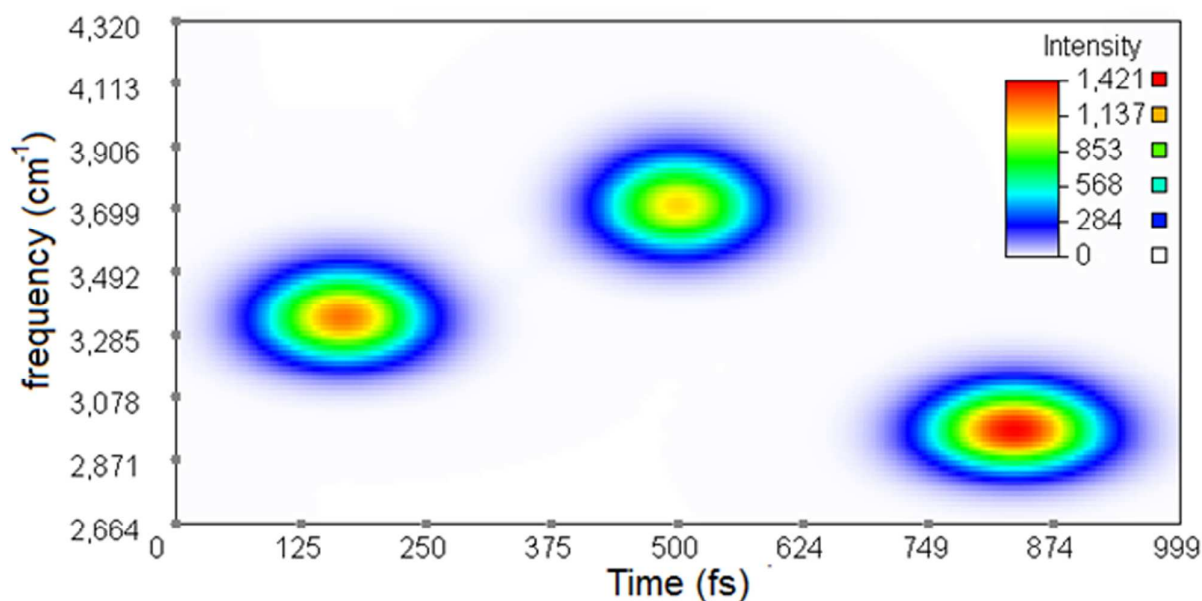


Figure 6. The time-resolved spectrum of sine waves shows three peaks at different time. The first peak at 166 fs is 3333 cm^{-1} , the second one at 500 fs is 3708 cm^{-1} , and the last one at 833 fs is 2958 cm^{-1} .

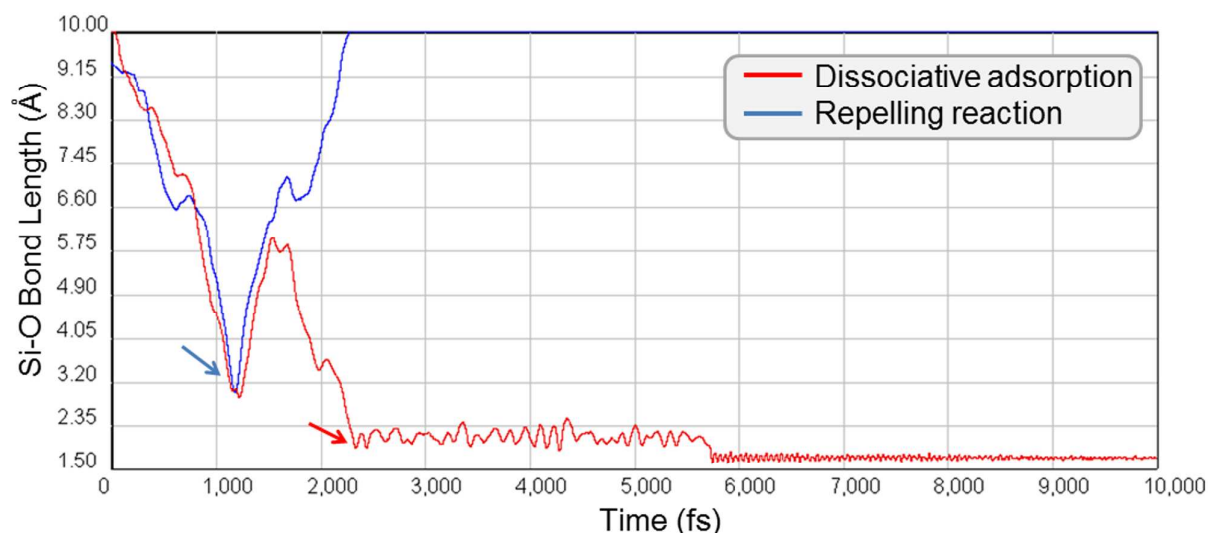


Figure 7. The trajectories of the Si-O bond length along the dissociative adsorption and repelling reaction are shown. Both red and blue arrows indicate the time at which the $\text{CH}_3\text{OH}_{(\text{g})}$ is attached to the surface.

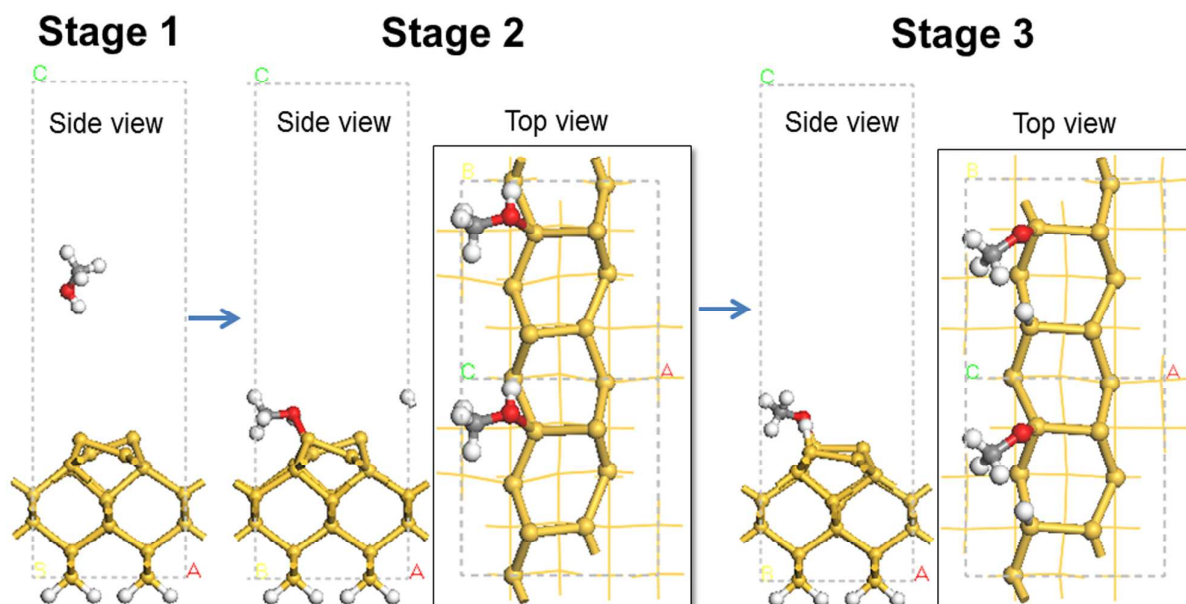


Figure 8. The structural models illustrate that (1) the $\text{CH}_3\text{OH}_{(\text{ads})}$ is translated toward the Si(001) surface at stage 1, (2) the O atom of the $\text{CH}_3\text{OH}_{(\text{ads})}$ bonds with the buckled-down Si atom at stage 2, and (3) both $\text{CH}_3\text{O}_{(\text{ads})}$ and $\text{H}_{(\text{ads})}$ species are adsorbed on the Si(001) surface subsequent to the O-H bond cleavage.

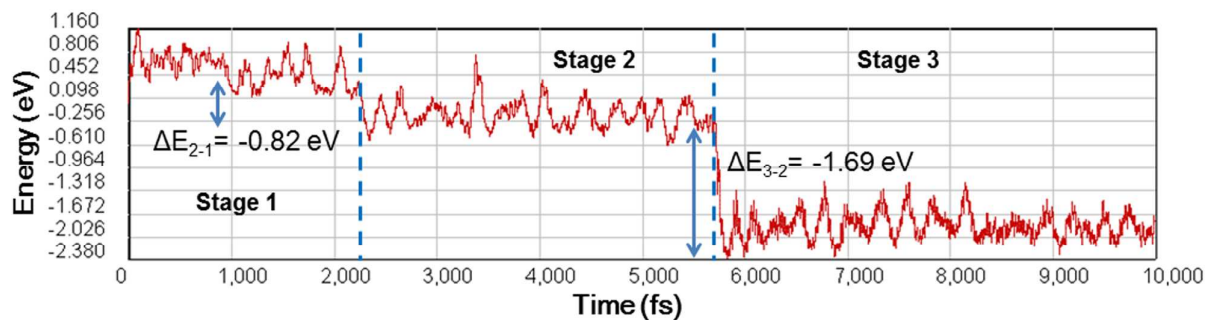


Figure 9. The total energy trajectory subtracted by that at the first step of the DFTMD simulation along the dissociative adsorption.

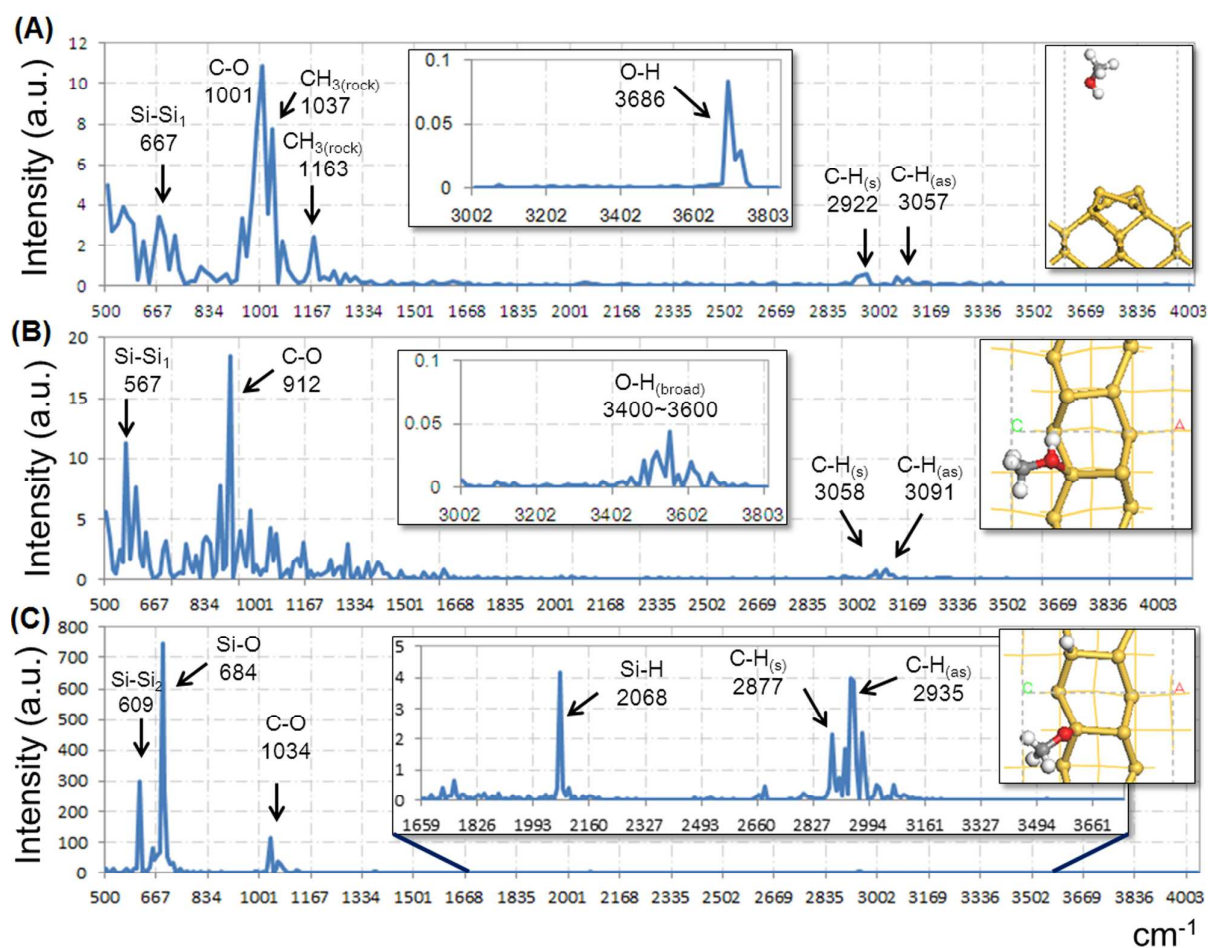


Figure 10. The calculated IR spectra at 3 stages, i.e. $\text{CH}_3\text{OH}_{(g)}$, $\text{CH}_3\text{OH}_{(ads)}$, and $\text{CH}_3\text{O}_{(ads)} + \text{H}_{(ads)}$ are shown, respectively. Based on the O-H dipole moment at stage 1 and stage 2, the IR peaks of the O-H stretching mode are shown in the both insets.

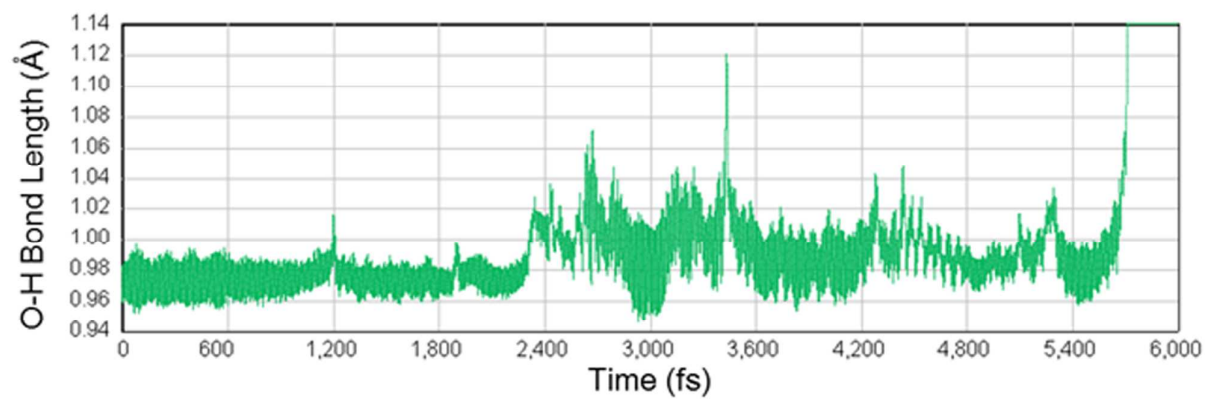


Figure 11. The trajectory of the O-H bond length along the dissociative adsorption from 0.0 ps to 6.0 ps is shown.

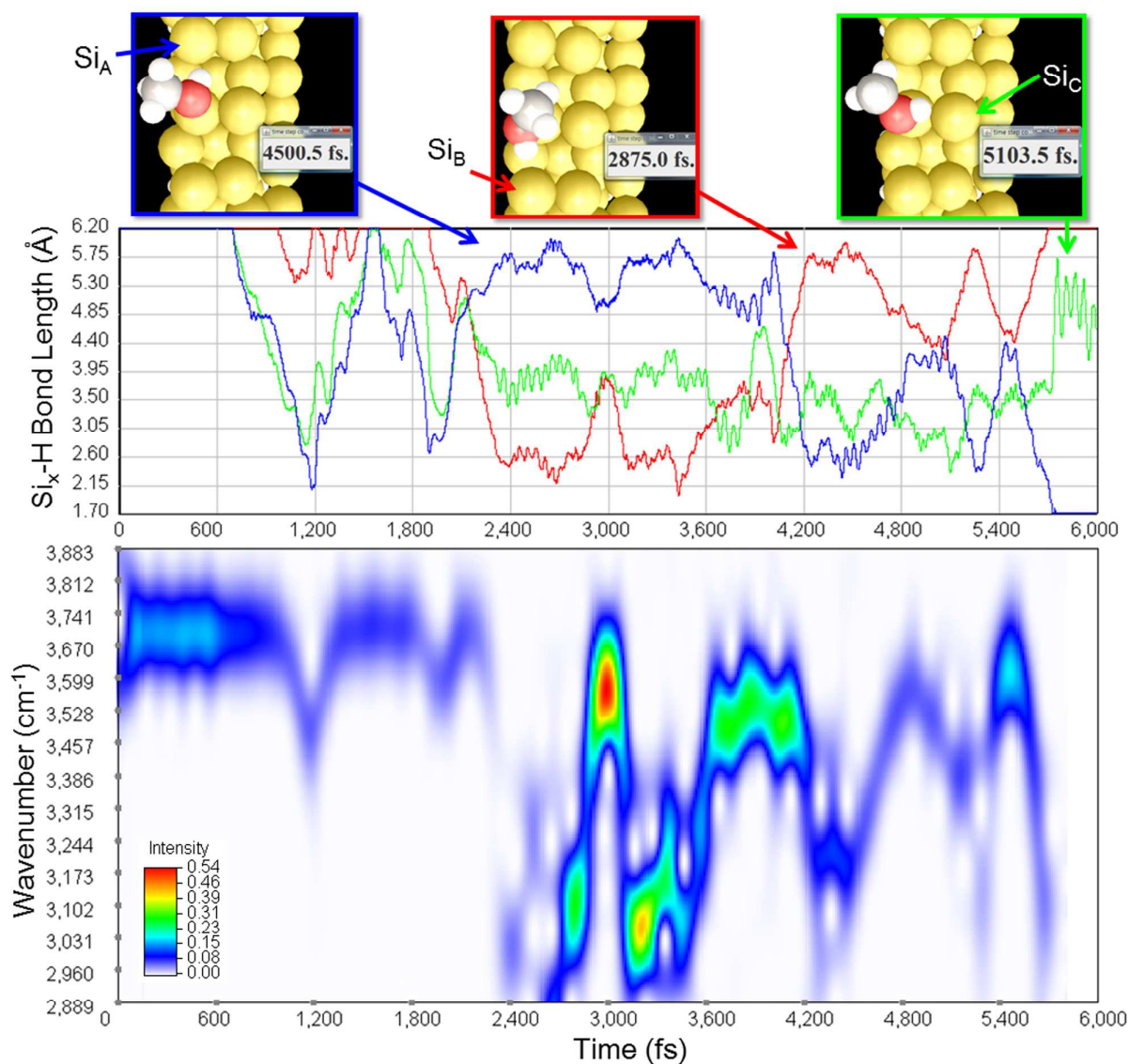


Figure 12. The distances between the H₂O atom and the buckled-up Si atoms are shown in the middle figure, and the time-resolved spectrum constructed by WT-SCAF is shown in the bottom figure.

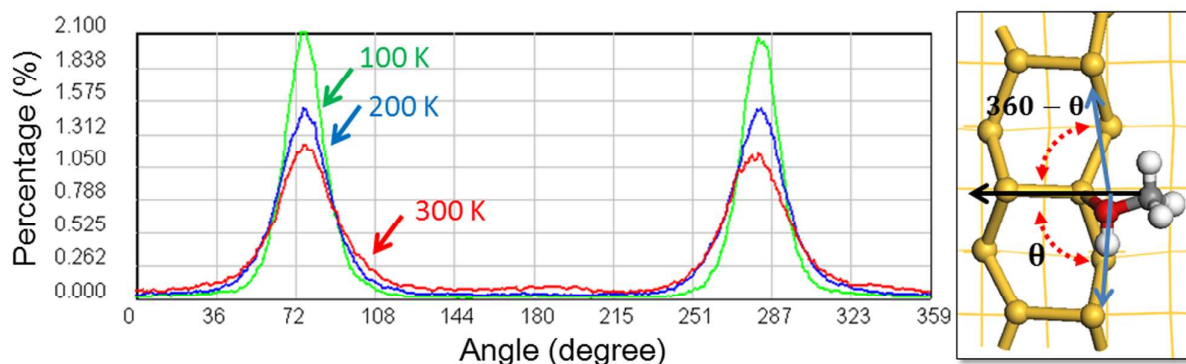


Figure 13. The distributions of the angle between the Si dimer and the O-H bond at 100 K (green line), 200 K (blue line), and 300 K (red line) are shown. In the structural figure, the black and blue arrows mean the vectors of the Si dimer and the O-H bond, respectively.

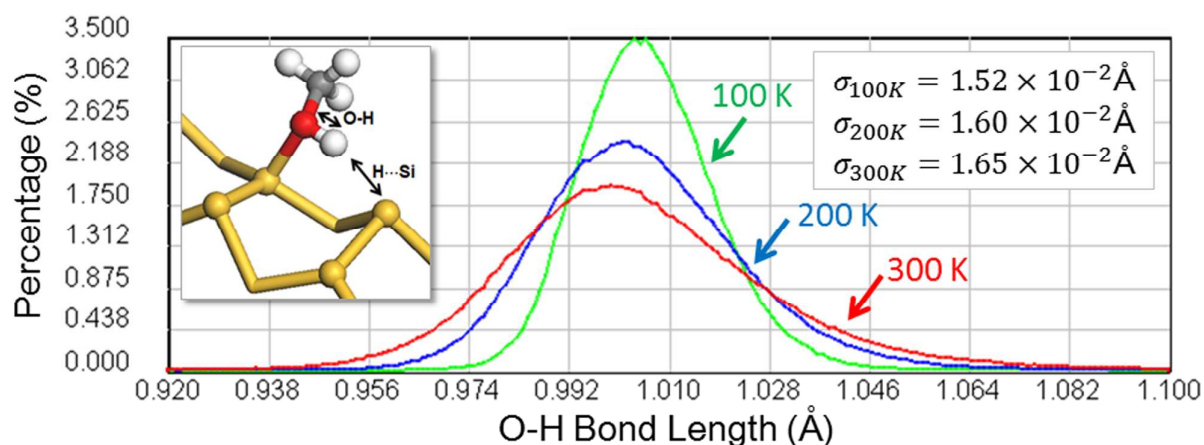


Figure 14. The distributions of the O-H bond length at 100 K (green line), 200 K (blue line), and 300 K (red line) are shown. The right inset indicates that the standard deviations of the O-H bond length at these temperatures are 0.0152 Å, 0.0160 Å, and 0.0165 Å, respectively.

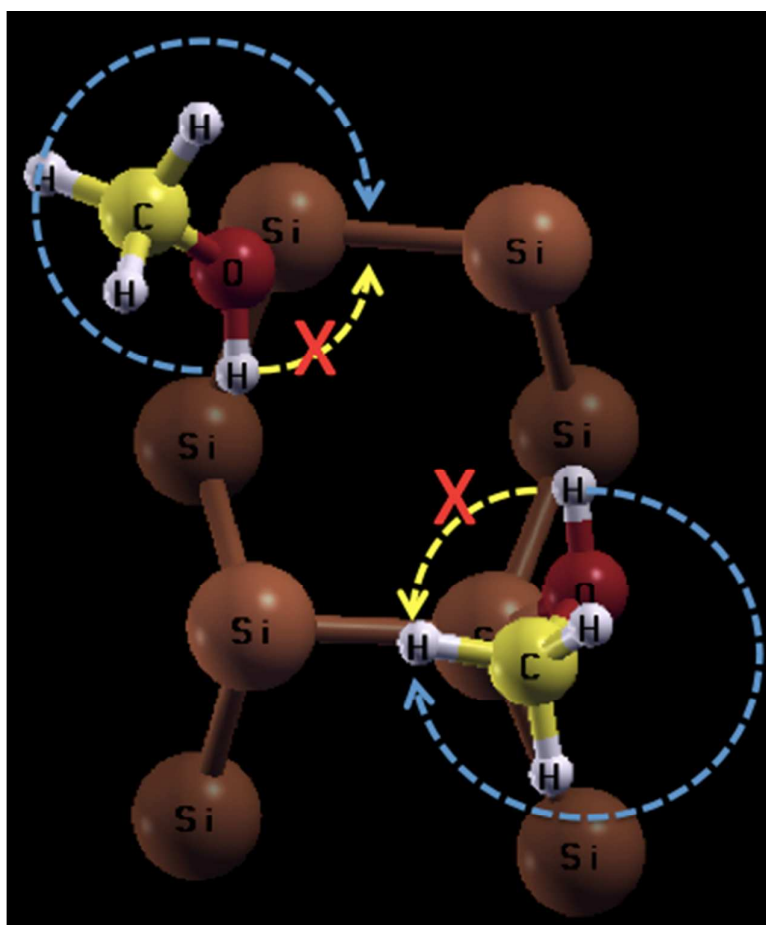


Figure 15. The structural model (top view) of two methanols adsorbed on the Si(001) surface. The dash-line with yellow color could be the constrained rotational range due to the repulsions between H_O atoms, while the dash-line with blue color could be the allowed rotational range of the O-H bond of the methanol adsorbed on the Si(001) surface.

Table 1. In the dissociative adsorption, the various bond lengths at three stages are listed, i.e. $\text{CH}_3\text{OH}_{(\text{g})}$, $\text{CH}_3\text{OH}_{(\text{ads})}$, and $\text{CH}_3\text{O}_{(\text{ads})}+\text{H}_{(\text{ads})}$.

Bond (Å)	O-H	O-C	C-H	O-Si	Si-H	Si-Si _{dimer 1}	Si-Si _{dimer 2}
$\text{CH}_3\text{OH}_{(\text{g})}$	0.974	1.442	1.1032	-	-	2.381	2.375
$\text{CH}_3\text{OH}_{(\text{ads})}$	0.994	1.474	1.0975	2.113	-	2.416	2.371
$\text{CH}_3\text{O}_{(\text{ads})}+\text{H}_{(\text{ads})}$	-	1.438	1.1039	1.697	1.524	2.447	2.393

Table 2: Total energies of optimized $\text{CH}_3\text{OH}_{(\text{ads})}$ on the Si(001) surface.

Adsorbed structures	Total energy (eV)
Type 1: The O-H bond pointing to the same buckled-up Si atom	-3341.335
Type 2: The O-H bond pointing to the adjacent buckled-up Si atom	-3341.363

Table 3. The counts of two reaction pathways and corresponding populations at 100 K, 200 K, and 300 K are listed. Total number of the DFTMD simulations at each temperature is 75.

Reaction pathways	Dissociative adsorption (a) Direct adsorption → (b) Dissociative reaction	Repelling reaction
100 K	75 (100.0 %) → 0 (0.0 %)	0 (0.0 %)
200 K	75 (100.0 %) → 0 (0.0 %)	0 (0.0 %)
300 K	74 (98.6 %) → 5 (6.7 %)	1 (1.3 %)

Table 4: Total energies of $\text{CH}_3\text{O}_{(\text{ads})}+\text{H}_{(\text{ads})}$ and $\text{CH}_2\text{OH}_{(\text{ads})}+\text{H}_{(\text{ads})}$ on the Si(001) surface.

Adsorption Site	Total energy of $\text{CH}_3\text{O}_{(\text{ads})}+\text{H}_{(\text{ads})}$ (eV)	Total Energy of $\text{CH}_2\text{OH}_{(\text{ads})}+\text{H}_{(\text{ads})}$ (eV)
H adsorbed on the same buckled-up Si atom	-3343.258	-3342.250
H adsorbed on the adjacent buckled-up Si atom	-3343.163	-3342.084

Table 5. The calculated IR spectra of methanol dissociative adsorption, corresponding experimental IR spectra, and normal mode calculations are listed.

Vibrational mode	The DFTMD simulation			Experimental IR spectra			Normal mode ¹¹	
	CH ₃ OH _(g)	CH ₃ OH _(ads)	CH ₃ O _(ads) +H _(ads)	CH ₃ OH _(g) NIST ³³	CH ₃ O _(ads) +H _(ads) at 150 K ⁶	C ₂ H ₅ OH _(ads) at 135 K / 219 K ⁷	CH ₃ OH _(g)	CH ₃ O _(ads) + H _(ads)
O-H	3685	3000~3600	-	3681	-	3267	-	-
C-H _(as)	3057	3068	2935	3000/2960	-	2983 _{CH3}	3007/2916	3001/2947
C-H _(s)	2922	2946	2877	2844	-	2881 _{CH2} /2928 _{CH3}	2876	2893
Si-H	-	-	2068	-	2090	2089	-	2127
C-H _(sci)	1434	1445	1442	1455	1454	1481	1452	1449
C-H _(rock)	1037/1117	1067/1122	1142	1060/1165	1169	-	1055/1135	1138/1164
C-O	1001	912	1034	1033	1050	-	1027	-
Si-O	-	-	684	-	-	756	-	742
Si-Si _{row 1}	667	567	-	-	-	-	-	-
Si-Si _{row 2}	-	-	609	-	-	-	-	-

Graphical Abstract

A novel theoretical study of thermally-induced reaction and vibration dynamics of methanol dissociative adsorption onto Si(001) surface

Yung Ting Lee and Jyh Shing Lin*

The thermally-induced reaction dynamics of methanol dissociative adsorption onto the Si(001) surface is studied by combining density functional theory-based molecular dynamics simulations with a molecular adsorption sampling scheme for investigating reaction pathways and corresponding infrared spectra. The main reaction pathway - dissociative adsorption - involves direct adsorption and dissociation adsorption process. According to structural analysis and spectrogram constructed by wavelet transform, the O-H dissociation of methanol occurs because of temperature rising and inductive effects by substrate.

